University of Jon Doe

**Thesis**

# Title of the thesis

**If you want you can have a subtitle**

Jon Doe

October 10, 2025

Prof. Dr. rer. LaTeX

# Contents

**List of Figures** . . . . . **I**

**List of Tables** . . . . . **II**

**List of Listings** . . . . . **III**

**1 Introduction** . . . . . **1**

**2 Experimental Section** . . . . . **3**

**3 Results** . . . . . **4**

3.1 Coin-cell cycling (Task 3.1) . . . . . 4

3.1.1 Potential–capacity profiles . . . . . 4

3.1.2 Incremental capacity (dQ/dE) analysis . . . . . 5

3.1.3 Coulombic efficiency . . . . . 6

**4 Conclusion** . . . . . **8**

**References** . . . . . **9**

# List of Figures

1 Potential *vs.* specific capacity at 0.1 C, 1 C and 2 C for the assembled coin cell. Higher C–rates exhibit increased polarization and reduced accessible capacity compared to 0.1 C. . . . . 4
2 Incremental capacity (dQ/dE) *vs.* potential at different C–rates. At 0.1 C, sharp, well–resolved peaks reveal distinct graphite staging transitions and NMC811 cathode redox processes. With increasing rate, peaks broaden and decrease in amplitude, with high–voltage features showing progressive suppression. . . . . 5

# List of Tables

3.1 Coulombic efficiency values for all cycles at different C–rates . . . . . 6

# List of Listings

# 1 Introduction

Lithium ion batteries (LIBs) have become the backbone of modern portable electronics and electric vehicles.[1] When Sony commercialized the first LIB in 1991,[2] it marked the beginning of a transformation in energy storage that would eventually earn Whittingham, Goodenough, and Yoshino the 2019 Nobel Prize in Chemistry.[1] The advantages of LIBs over earlier rechargeable systems (higher energy and power densities, higher operating voltages, and longer cycle life)[2] have made them the dominant technology in today's applications.

The basic operating principle of a LIB involves two intercalation electrodes (anode and cathode) separated by a lithium-ion conducting electrolyte and porous separator. During discharge, $Li^+$ ions leave the graphite anode and travel through the electrolyte to the cathode (typically a lithium metal oxide), while electrons flow through the external circuit; charging reverses this process. Graphite has emerged as the standard anode material because it accommodates $Li^+$ ions between its graphene layers (forming $LiC_6$) with relatively little structural change. However, the low potential of lithiated graphite lies outside the electrochemical stability window of most organic electrolytes, which leads to electrolyte decomposition and formation of a solid electrolyte interphase (SEI) on the anode surface. This nanoscale passivation layer blocks electron transport while allowing $Li^+$ ions to pass through, though its initial formation irreversibly consumes some lithium. Despite this cost, the SEI prevents ongoing electrolyte breakdown and is critical for long-term battery stability.[1]

Battery performance, internal resistance, and lifetime all depend heavily on these interfacial processes (SEI formation, charge-transfer kinetics, and ionic transport through the electrolyte). Increasing interfacial resistance or persistent side reactions (such as electrolyte decomposition or electrode degradation) gradually reduce battery capacity by consuming active lithium and raising internal resistance.[1]

A range of electrochemical characterization techniques exist to probe these interfacial processes. Cyclic voltammetry (CV) measures current as a function of swept voltage, revealing redox reactions and their reversibility. A reversible redox process produces symmetric oxidation and reduction peaks whose separation and shape reflect Nernstian equilibrium and diffusion effects, while kinetic limitations cause peak shifts and distortion.[3]

Galvanostatic charge–discharge testing (cycling at constant current) remains the standard technique for evaluating battery capacity, energy efficiency, and rate capability. These measurements yield specific capacity (mAh $g^{-1}$) and Coulombic efficiency (the discharge-to-charge capacity ratio) for each cycle.

Electrochemical impedance spectroscopy (EIS) takes a different approach by applying small AC perturbations across a range of frequencies. This technique excels at separating different interfacial processes by fitting the measured impedance to equivalent circuit models. The high-frequency intercept in a Nyquist plot typically corresponds to electrolyte resistance, while mid- to

low-frequency features (semicircles or Warburg slopes) reflect double-layer capacitance, charge-transfer resistance, and diffusion impedance. Fitting these spectra extracts quantitative parameters like charge-transfer resistance, exchange current, and diffusion coefficients. Unlike large-perturbation methods, EIS operates near equilibrium, which allows precise characterization of both fast and slow processes.[4]

Together, voltammetric, galvanostatic, and impedance techniques provide complementary insights into electrochemical interfaces, identifying thermodynamic, kinetic, and transport properties.

# 2 | Experimental Section

# 3 | Results

## 3.1 Coin-cell cycling (Task 3.1)

### 3.1.1 Potential–capacity profiles

Figure 1 overlays the specific capacity *vs.* potential curves at the three C–rates. At the low rate (0.1 C), the discharge capacity is highest and the (de)lithiation plateaus are most clearly developed. With increasing rate (1 C and 2 C), polarization grows (larger charge–discharge hysteresis) and the accessible capacity decreases, consistent with kinetic and transport limitations. The chosen voltage window (2.4 V to 4.2 V) spans the practical operating region of the NCM 811 | graphite full cell; at low rate it enables utilization of most of the available capacity, while at higher rates kinetic limitations dominate the accessible capacity.

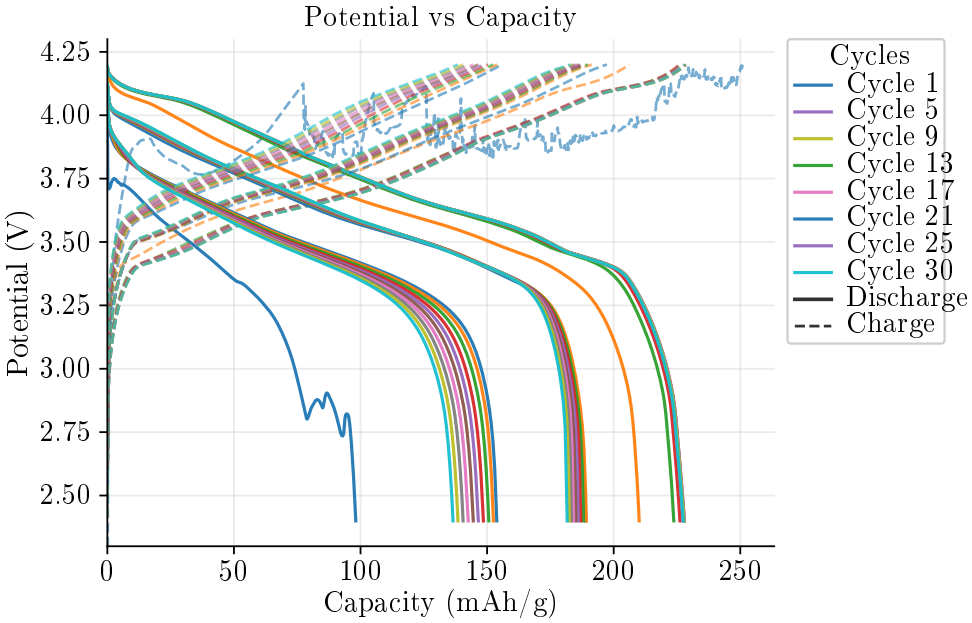


**Figure 1:** Potential *vs.* specific capacity at 0.1 C, 1 C and 2 C for the assembled coin cell. Higher C–rates exhibit increased polarization and reduced accessible capacity compared to 0.1 C.

The experimental discharge capacities at 0.1 C reach approximately 227 mAh/g, which compares favorably to the theoretical capacity of graphite (372 mAh/g for $LiC_6$ formation). The capacity shows a clear dependence on C–rate, with decreasing accessible capacity at higher rates due to kinetic limitations and increased polarization.

### 3.1.2 Incremental capacity (dQ/dE) analysis

The cathodic incremental capacity analysis reveals distinct electrochemical processes at each C–rate.

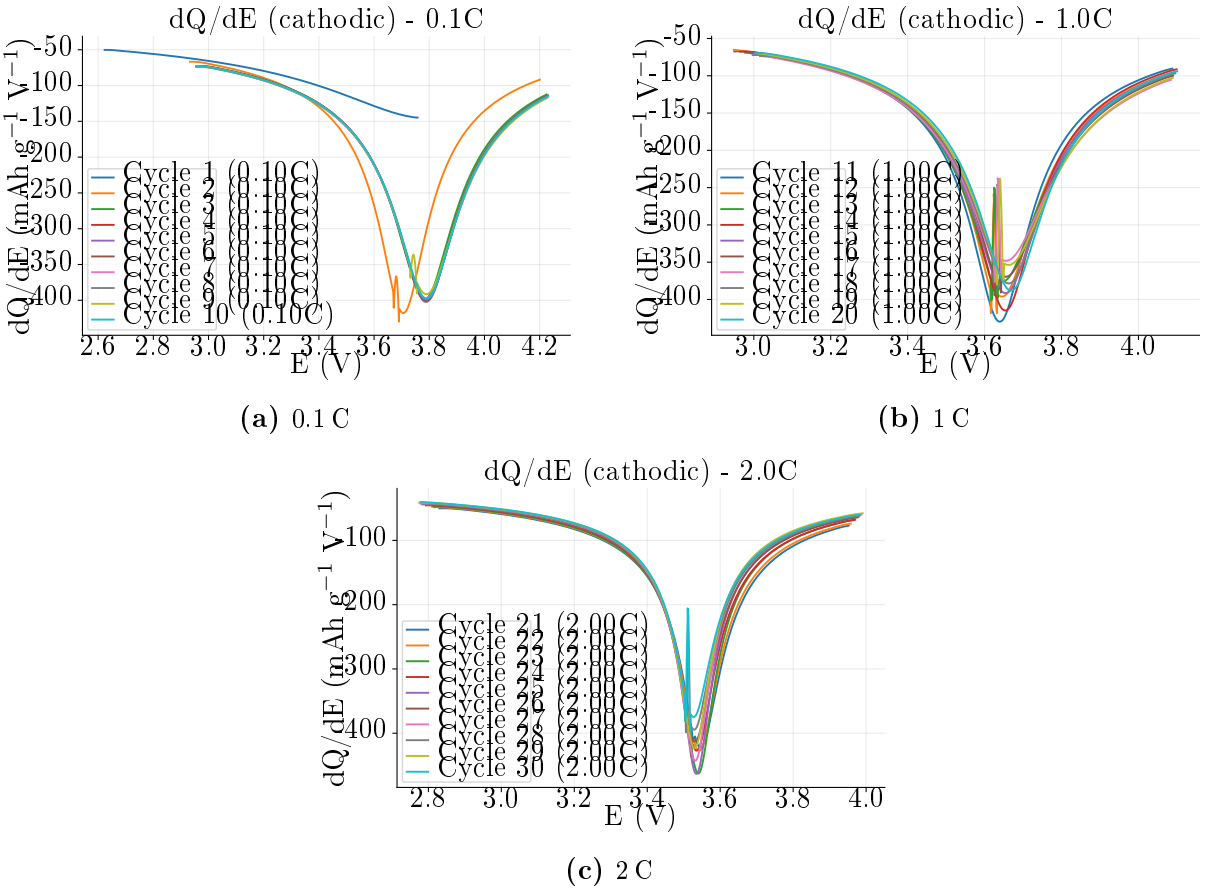


**(a)** 0.1 C **(b)** 1 C

**(c)** 2 C

**Figure 2:** Incremental capacity (dQ/dE) *vs.* potential at different C–rates. At 0.1 C, sharp, well–resolved peaks reveal distinct graphite staging transitions and NMC811 cathode redox processes. With increasing rate, peaks broaden and decrease in amplitude, with high–voltage features showing progressive suppression.

Figure 2a shows the 0.1 C discharge profile, where several sharp, well–resolved peaks appear between 3.0–4.1 V. A dominant group around 3.4–3.8 V corresponds to staged $Li^+$ intercalation in graphite (progression toward stage 1, $LiC_6$), while a shoulder near 3.9–4.1 V reflects the high–voltage redox of the NMC811 cathode. These features align with the plateaus observed in Figure 1.

At 1 C (Figure 2b), the peaks begin to broaden and decrease in amplitude, with the highest–voltage features showing the most significant suppression. The graphite staging peaks remain discernible but are less sharp, indicating increased kinetic limitations while maintaining reasonable reversibility.

The 2 C profile (Figure 2c) demonstrates substantial peak broadening and amplitude reduction. The high–voltage cathode features are largely suppressed, and the graphite staging peaks merge

into broader features, reflecting transport–limited behavior at this rate.

From these individual rate analyses we conclude that rate–induced polarization progressively dominates with increasing C–rate, merging graphite staging peaks and suppressing high–voltage features. No additional peaks emerge at high rate within 2.4–4.2 V, consistent with the high Coulombic efficiency and absence of parasitic processes. Graphite intercalation steps remain discernible up to 1 C, indicating acceptable anode kinetics; at 2 C they become transport–limited.

### 3.1.3 Coulombic efficiency

The Coulombic efficiency (CE) was evaluated as the ratio of discharge to charge capacity for each cycle using Equation 3.1:

$$CE = \frac{Q_{discharge}}{Q_{charge}} \times 100\% \tag{3.1}$$

The CE values from the cycling data show distinct behavior at different C–rates. Table 3.1 presents the complete CE data for all cycles at each C–rate.

**Table 3.1:** Coulombic efficiency values for all cycles at different C–rates

**(a)** 0.1 C

| Cycle | CE (%) |
|---|---|
| 1 | 39.1 |
| 2 | 101.8 |
| 3 | 98.8 |
| 4 | 100.1 |
| 5 | 100.0 |
| 6 | 99.9 |
| 7 | 99.7 |
| 8 | 99.7 |
| 9 | 99.7 |
| 10 | 99.7 |

**(b)** 1 C

| Cycle | CE (%) |
|---|---|
| 11 | 95.7 |
| 12 | 98.9 |
| 13 | 99.1 |
| 14 | 99.1 |
| 15 | 99.1 |
| 16 | 99.2 |
| 17 | 99.2 |
| 18 | 99.2 |
| 19 | 99.3 |
| 20 | 99.3 |

**(c)** 2 C

| Cycle | CE (%) |
|---|---|
| 21 | 98.7 |
| 22 | 99.0 |
| 23 | 98.9 |
| 24 | 98.8 |
| 25 | 98.8 |
| 26 | 98.7 |
| 27 | 98.6 |
| 28 | 98.6 |
| 29 | 98.6 |
| 30 | 98.6 |

At 0.1 C, the initial cycle shows a low CE of 39.1% due to SEI formation and initial activation processes. However, subsequent cycles rapidly stabilize with CE values approaching 100% (cycles 2–10: 98.8–100.1%), indicating excellent reversibility once the SEI is established.

At 1 C, the CE remains consistently high throughout cycling (95.7–99.3%), with slight variations attributed to increased polarization effects. The 2 C rate shows similar high CE values (98.6–99.0%), demonstrating that the cell maintains good reversibility even at elevated current densities.

The CE shows minimal dependence on C–rate once the initial formation cycles are completed, indicating that the chosen voltage window (2.4–4.2 V) allows for stable operation across all tested rates without significant side reactions or electrolyte decomposition.

# 4 Conclusion

# References


(1) Goodenough, J. B.; Park, K.-S. The Li-Ion Rechargeable Battery: A Perspective. *Journal of the American Chemical Society* **2013**, *135*, 1167–1176.

(2) Van Noorden, R. The rechargeable revolution: A better battery. *Nature* **2014**, *507*, Request PDF: `https://www.researchgate.net/publication/260562281_The_rechargeable_revolution_A_better_battery`, 26–28.

(3) Elgrishi, N.; Rountree, K. J.; McCarthy, B. D.; Rountree, E. S.; Eisenhart, T. T.; Dempsey, J. L. A Practical Beginner's Guide to Cyclic Voltammetry. *Journal of Chemical Education* **2018**, *95*, 197–206.

(4) Lazanas, A. C.; Prodromidis, M. I. Electrochemical Impedance Spectroscopy—A Tutorial. *ACS Measurement Science Au* **2023**, *3*, 162–193.